Tata Institute of Fundamental Research

Graduate School Project Report

Microscopic Characterization of Hybrid Photo Diode

Author:
Mohit Saharan
DHEP, TIFR, Mumbai

Supervisor:
Prof. Shashi R. Dugad
DHEP, TIFR, Mumbai

January 1, 2019

Abstract

CMS Hadron End-Cap Calorimeter(HE) data indicated loss in signal due to damage of scintillators and Hybrid Photo Diodes(HPDs). Microscopic characterization of HPD decommissioned from HE detector has been carried out to find out the contribution of HPD to net signal loss. Position dependent current response was measured with a step size of 75 μm along transverse axes. Very fine regions of photocathode was illuminated with a focussed laser beam of wavelength = 520 nm, and spot size between 1.7 μm and 6.2 μm. Photocathode showed non-uniform response and signs of localized damage in the form of circular spots, caused by excessive illumination. HPD showed a maximum signal loss of 60.8%. The magnitude of threshold voltage of damaged region was found to be 531 Volts higher than that of undamaged region.

Contents

1 Introduction

The CMS detector is designed to study a wide range of fundamental problems involving diverse signatures with final states containing muons, electrons, photons, hadron jets, and neutrinos or exotic particles resulting in apparent missing energy[3]. CMS is made up of several sub-detectors[2]: Silicon Tracker, Electromagnetic Calorimeter, Hadron Calorimeter (HCAL), and Muon Chamber. The HCAL is further divided into four parts: Hadron Barrel Calorimeter (HB), Hadron Outer Calorimeter (HO), Hadron Forward Calorimeter, and Hadron End–Cap Calorimeter (HE). The HB and HE are made up of alternating layers of absorber (brass) and scintillator and the detector is segmented into $\eta - \phi$ towers, where η is pseudorapidity, defined as,

$$\eta = -ln(tan\frac{\theta}{2})$$

where, θ is the polar angle between the tower and the beam axis and ϕ is the azimuthal angle. The HB and HE jointly covers the pseudorapidity in the range of $|\eta| = 0 - 3$. The granularity of segments is $\Delta\eta \times \Delta\phi = 0.087 \times 0.087$ for $|\eta| < 1.6$ and $\Delta\eta \times \Delta\phi = 0.17 \times 0.17$ for $|\eta| \geq 1.6$ [3]. The scintillation light produced in the HCAL is collected by the wavelength shifting fibers (WLS), which are embedded in the scintilator tiles. From WLS fibers, the light is further transported via clear fibers to an Optical Decoding Unit (ODU)[2]. The ODU bunches the fibers coming from the same tower and maps them onto the designated photodetector (HPD).

Over the years, the loss in signal was observed in the HE detector data and the loss became more prominent with increasing luminosity. The degradation was expected due to exposure of the scintillators and photodiodes of this region to very high radiation[1]. Various in-situ studies were carried out to find the radiation damage to this detector. Signal loss was reported in all the studies but none of them were able to decouple the individual contribution of HPDs and the scintillator to net signal loss. Since the HPDs were easily accessible, some HPDs were decommissioned from CMS to study them seperately. TIFR took the responsibility of studying these detectors microscopically since the SIPM group has a unique microscopic characterization facility. The Micron Resolution Optical Scanner (MROS)[5] was specially designed and built to study the microscopic characterization of photodetectors such as silicon photomultipliers. Effectiveness of MROS had been already demonstrated to study the SIPM microscopically. Therefore, two decommissioned HPDs (one from HO and another from HE) were sent to TIFR to carry out the study of their characteristics.

The MROS provides a focused beam of light on target. The mounting table which holds HPD can move in an automated manner in three orthogonal directions with a resolution of 0.1 μm with a dynamic range of 25 mm, which can scan almost whole of the active region of HPD [1]. Active region of HPD has a hexagonal shape with common photocathode. Underneath photocathode, there are nineteen hexagonal PIN diodes referred to as pixels. Each of the pixels have a seperate output. Using this setup, an extensive characterization of the HPD obtained from HE detector has already been carried out by R. Shukla et al.[1] This study verifies the result and is an extension to their work.

The study has revealed significant localized damaged to the photocathode of the HPD. The damage to the photocathode is prominent in the region exposed to the optical fiber and is less visible in the neighboring region. The damage to HPD was expected to manifest in the form of increase of threshold voltage in the damaged regions. Therefore, the threshold voltage analysis was carried out to see the variation of threshold voltage in

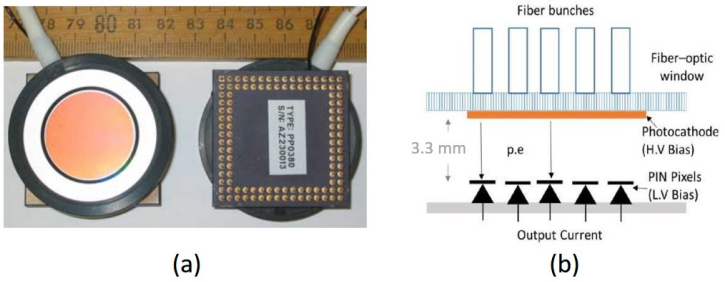

Figure 1: a) Picture of HPD showing it's physical dimensions [4], b) Schematic of HPD [1]

different regions of HPD. The difference between the threshold voltage of damaged region and undamaged region(average of 25 randomly chosen points) is found to differ by 531 Volts. The conductance of the photocathode is found to increase with the decreasing exposure to scintillation light.

2 Hybrid Photo Diode

HPDs were installed in CMS because they have high gain and immunity to magnetic field when aligned to HPD axis. The HPDs were designed to operate for 10 years in the CMS experiment corresponding to an integrated charge intensity of 3 C/pixel [1] at the highest pseudorapidity locations. The physical dimensions of HPD are shown in Figure 1(a).

Figure 1(b) shows the schematic of HPD. The photocathode is covered by a fiber optic window. Underneath photocathode, there are nineteen PIN diodes of hexagonal shape and 5.4 mm in size, referred as pixels. All the PIN diodes have a seperate output. The photocathode is reverse biased by applying a very high voltage (V_{gap} = -6 kV to -10 kV) across the 3.3 mm gap. The PIN diodes are reverse biased by applying a low voltage of -80 volts.

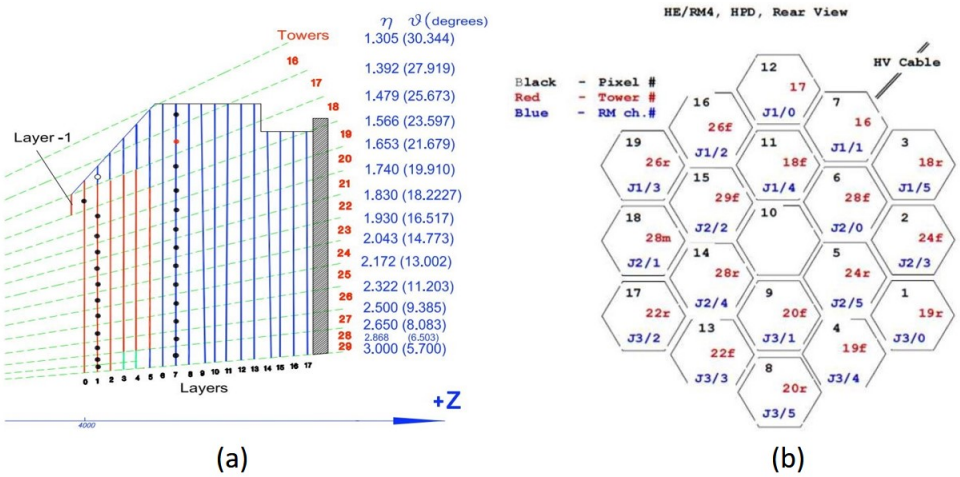

Figure 2: a) Geometrical Schematic of the towers in the HE detector[1], b) Mapping of HE towers onto the HE-HPD[1]

The HE is divided into $\eta - \phi$ towers of granularity $\Delta\eta \times \Delta\phi = 0.087 \times 0.087$ for $|\eta| < 1.6$ and $\Delta\eta \times \Delta\phi = 0.17 \times 0.17$ [3]. Figure 2(a) shows the segmentation of HE.

Each vertical line represents the scintillator layer and the lines going from left to right are the towers, numbered from 16 to 29. Furthermore, it is segmented into three regions: forward, middle, and rear. In Figure 2(a), forward region is shown in orange color, rear region is shown in blue color, and the middle region consists of two scintillator layers only (layer no. 3 and 4 in the tower 28 and 29).

For ease of data collection in HCAL, every scintillator layer is divided into sections called trays [2]. The trays are further divided into scintillator tiles. The $\eta - \phi$ dimensions of every tile are same as that of a tower. During data collection, light from every tile is collected by a WLS fiber. WlS fiber collects the blue light from scitillator and converts it into blue light. The WLS fibers are spliced with clear fibers (which have a higher attentuation length), at the end of tray. Clear fibers transport the light to HPDs which are located far from the scintillator tray. The Optical Decoding Unit arranges these clear fibers coming from the same towers into bundles and maps the bundle onto designated HPD. Figure 2(b) shows the mapping of the towers for the HPD used in this study.

3 Experimental Setup

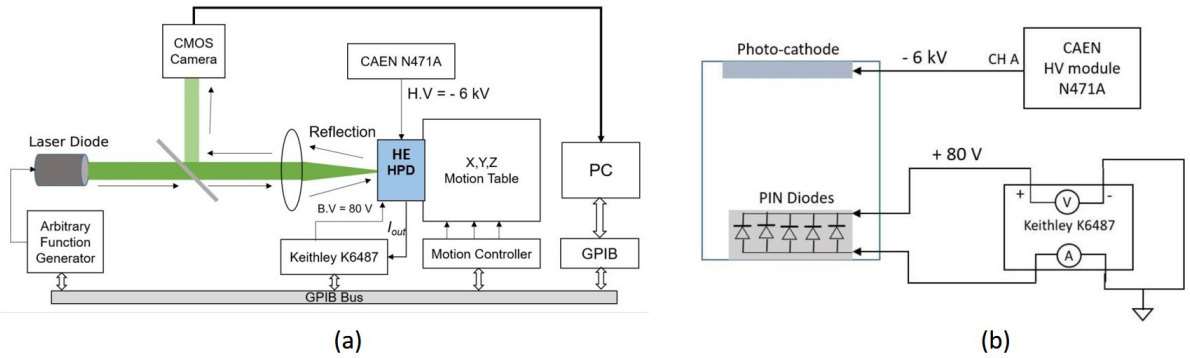

Figure 3: a) Schematic of experimental setup [1], b) Schematic showing electrical connections of power supply [1]

A schematic of the experimental setup is shown in Figure 3(a). Since the HPDs are primarily exposed to the green light coming from scintillator, a green laser (wavelength = 520 nm) was used in this study. The laser intensity was kept low during the scans to avoid any possible damage of the photocathode during long runs. Function generator was used to power the laser. The laser was operated in CW mode (frequency = 1kHz, amplitude = 1.6 V - 1.7 V, and duty cycle = 99.999%). The Keithley power supply (Keithley K6487) was used to reverse bias the PIN diodes (-80 V) and CAEN HV module N471A was used to reverse bias the photocathode(-6000V). This combination yields a large gain of about 2000 with low noise [1]. The HPD is mounted on the motion table which can be moved in an automated manner with a resolution of 0.1 μm [1] by a motion controller. The MROS is also equipped with a CMOS camera which helps in carrying out visual inspection of the surface of HPD, as well as in selecting a particular region of interest to be scanned. The setup was controlled through GPIB interface under LABVIEW based framework.[5]

Figure 3(b) shows schematic of the electrical connections of power supply. Since it was not needed to read the individual output of each pixel, the 19 output channels of HPD were read collectively as a single channel. The laser beam illuminates a very fine region

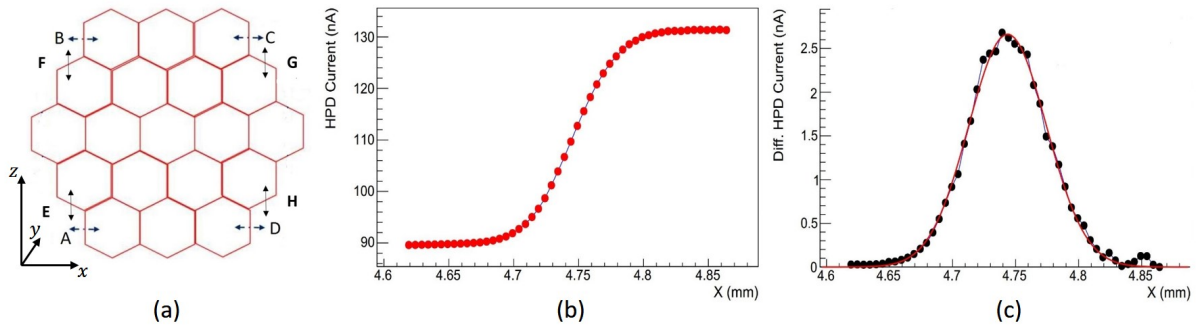

Figure 4: a) Focal scan positions and the chosen coordinate system, b) Variation of current with position, c) Variation of $\frac{dI}{dx}$ with x, when beam spot moves from dead region to active region

of the photocathode with MROS setup, therefore the recorded current would be because of the illuminated region only. Hence, reading the collective current does not affect the results.

4 Focal Plane Determination

Probing the microscopic regions on the surface of HPD requires a very fine beam spot size and alignment of HPD surface with the focal plane of laser beam. The MROS setup had been shown, using knife edge method, to be capable of producing a focused beam of spot size = 1.7 μm.[5] The alignment of focal plane of laser beam with the surface of HPD was done using the modified knife edge method.[1] In the knife edge method, a sharp edge is introduced in the path of the laser beam gradually to block the light falling on the photodetector. In the modified knife edge method, the boundary between the dead and active region on HPD acts as the edge. The HPD itself is moved gradually into the path of beam and the active region receives a varying amount of light depending on the position of HPD (Figure 4(a)). Current increases rapidly as the spot transitions into the active region and saturates when the spot lies completely into the active region. The typical form of variation of current with position is shown in the Figure 4(b). The variation of $\frac{dI}{dx}$ vs x is shown in Figure 4(c). The RMS of this Gaussian distribution is equal to the spot size of the beam [5]. The coordinate system used is shown in Figure 4(a).

A preliminary survey of the surface was been done (in earlier study [1]), before doing the actual scan, with the CMOS camera of MROS. Using that, a rough estimate of the focal plane was obtained. Some variation in the focal plane was observed over the surface because of mounting imperfections. Using modified knife edge method, the focal plane was accurately determined for various positions shown in Figure 4(a). Later in the surface scans, the focal axis of HPD was dynamically adjusted to keep the focal plane aligned with the surface of HPD. Here, the procedure of determining the focal plane is shown for position A and C.

A starting point(x,y,z) (obtained from the preliminary scan) was chosen near the mentioned positions (Figure 4(a)). Focal axis coordinate (y) was varied about the expected focal plane position in 12 steps with a step size of 20 μm. For each value of y, 50 steps (step size = 5 μm) were taken along x and current was measured at every position. Therefore, for each value of y, the beam spot size was calculated. Figure 4(b) shows the typical form of I vs x when y was far from focus, and Figure 5(a) shows the form of the variation

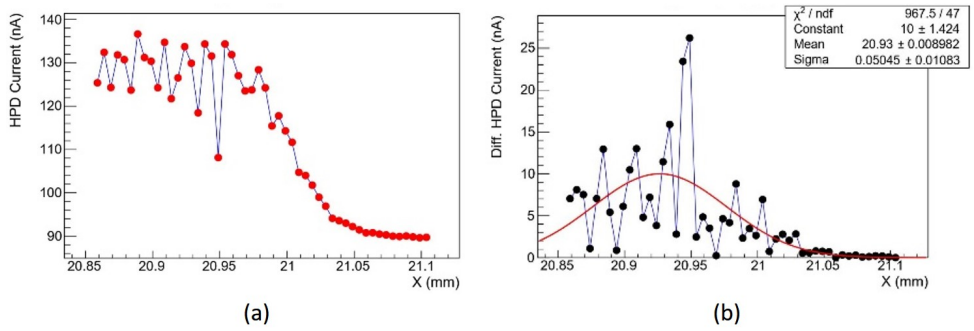

Figure 5: Plot of I vs x, and $\frac{dI}{dx}$ vs x for y which is a) far from focus, b) very close to focus

of I vs x when y was closest close to focus.

For the value of y which was closest to focal plane, HPD current and hence $\frac{dI}{dx}$ showed rapid variation with position. The row scan data corresponding to this particular y was not used to calculate the beam spot size (step 7 of position A and step 6 of position C in the table 1 are absent). The rapid variation of current with position is explained in section 5. The data from table 1 was fitted to the function [5]:

$$\sigma(y - y_o) = \sigma_o \times \sqrt{1 + \frac{(M^2\lambda(y - y_o))^2}{(4\pi{\sigma_o}^2)^2}}$$

where,
λ is the wavelength of the laser beam (520 nm)
M is beam quality factor
σ_o is the minimum beam spot size
σ is the beam spot size at a distance y - y_o relative to minima
y_o is the position of HPD corresponding to the minimum beam spot size

The parameters: M, σ_o, and y_o were determined by fitting the data shown in the table 1. Figure 6 shows the fitted plot of data shown in table 1. M = 13.5 for both position A and B. The focal plane for position A and C were found to be at y = 12.32 mm and y = 12.14 mm respectively.

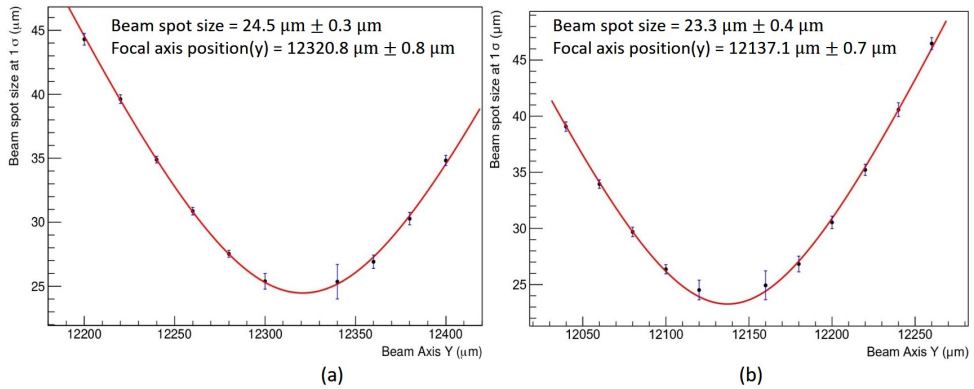

Figure 6: Plot of beam spot size vs y for position a) A, b) C

The minimum beam spot size obtained from the plots is much greater than the beam spot size that was stated earlier (1.7 μm). These numbers are different because of the

Steps along Y	Beam spot size (μm)	Std. Dev. (μm)
Position A		
1	44.3	0.5
2	39.6	0.3
3	34.9	0.3
4	30.7	0.3
5	27.5	0.3
6	25.4	0.6
8	25.4	1.4
9	26.9	0.5
10	30.3	0.5
11	34.8	0.4
12	40.1	0.5
Position C		
1	39.0	0.4
2	33.9	0.4
3	26.7	0.4
4	26.4	0.4
5	24.5	0.9
7	24.9	1.3
8	26.8	0.7
9	30.5	0.6
10	35.2	0.5
11	40.6	0.6
12	46.5	0.5

Table 1: Beam spot size corresponding to the row scans at position A and C

alternative of knife edge that was used here, the boundary between HPD's active and dead region. The response of the semiconductor edge was not as sharp as that of a knife edge and hence, it makes the beam spot size look broader in data. However, this does not affect the determination of focal plane of HPD. In next section, it will be shown that the beam spot size is indeed less than what we obtained from this data. Table 2 shows the coordinate of the focal plane for all the positions. The values of focal plane for positions other than A and C are taken from earlier study.[1]

Position	A	B	C	D	E	F	G	H
Focal Plane (y, mm)	12.32	12.26	12.14	12.22	12.32	12.26	12.14	12.18

Table 2: Coordinates of focal plane for all positions

5 Ultra-Fine Scan

In the previous section, it was observed that when the HPD's surface was aligned with the focal plane of the laser beam, then the current varied very rapidly with position. To investigate more into that, an ultra-fine scan of a small region of HPD (near position A)

was done while keeping it at exact focus. The scan covered an area of 100 μm $\times$ 97 μm with a step size of 1 μm along the transverse axes. The result of the scan is shown in Figure 7(a).

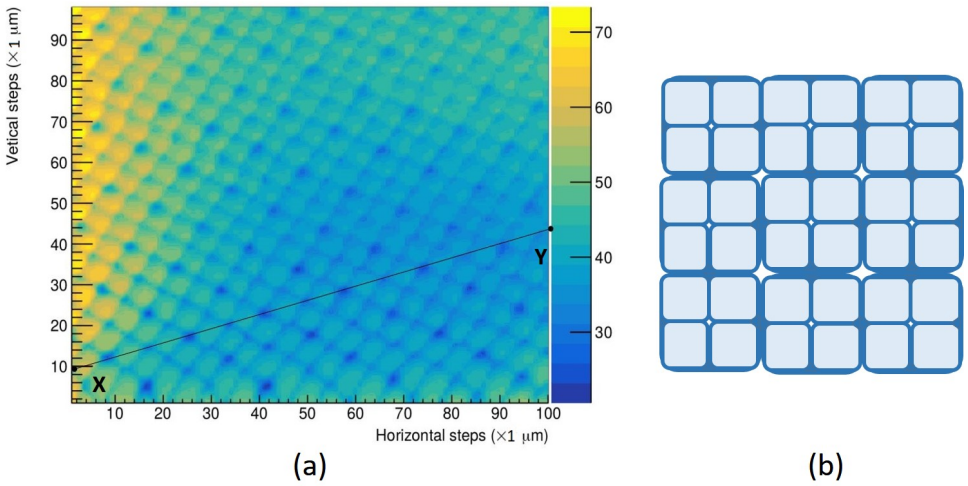

Figure 7: a) Ultrafine scan of HPD surface with a step size of 1 μm, b) Hypothetical structure of fiber-optic window

It has been hypothesized in this study that the structure of the fiber optic window is as shown in Figure 7(b). The laser beam, when passed over the edges and the vertices of the square shaped units (called as cell in further discussion), the light got partially blocked by the walls and hence these positions recorded a relatively lower current. These features were seen here only because the beam spot size was smaller than the size of the cell. Because of presence of fiber optic window above photocathode, we cannot say if the spot illuminating the photocathode had was exactly = 1.7 μm in size. But from Figure 7(a), it is clear that the beam spot size was less than the size of the cell. To find the size of the cell, moving along the line XY (Figure 7(a)) the variation of current with distance (in the unit of steps) w.r.t the point X was plotted.

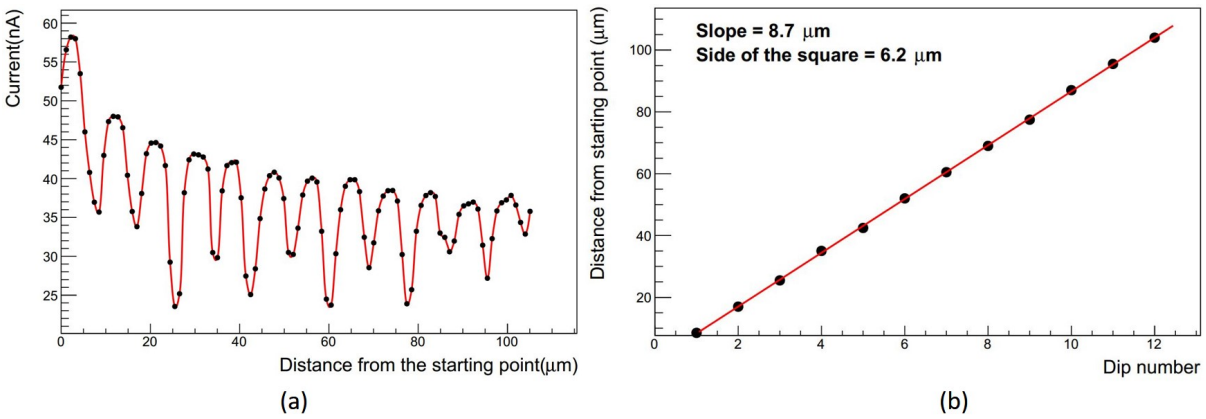

Figure 8: a) Variation of current along the line XY w.r.t distance from X, b) Distance from X vs dip number

X_o(0,7) and Y_o(91,38) were initially chosen to be the end points of the line(slope = 0.33735). To ensure that the line with the best features is obtained, ten more lines were

chosen. In all of these lines, X_o was kept unchanged and Y_o was changed. In five lines, the point Y_o was shifted up along vertical axis by 1,2, ... ,5 units relative to X_oY_o. For the other five lines, the Y_o was shifted down along vertical axis by 1,2, ... ,5 units relative to X_oY_o. The plot corresponding to the best line (XY) among those lines is shown in Figure 8(a).

The slope of the graph showing the dip number vs the distance (Figure 8(b)), gives the distance between two dips. Therefore, the distance between the two dips = 8.7 μm. Hence, the characteristic size of the cells = 6.2 μm, and the spot size of the beam was somewhere between 1.7 μm and 6 μm.

6 Surface Scans of HPD

The active region of HPD was scanned to see the current response of the photocathode. The laser was operated in CW mode (frequency = 1 kHz, amplitude = 1.65 V, duty cycle = 99.999%). The photocathode and PIN diodes was reverse biased by applying -6000 V and -80 V respectively.

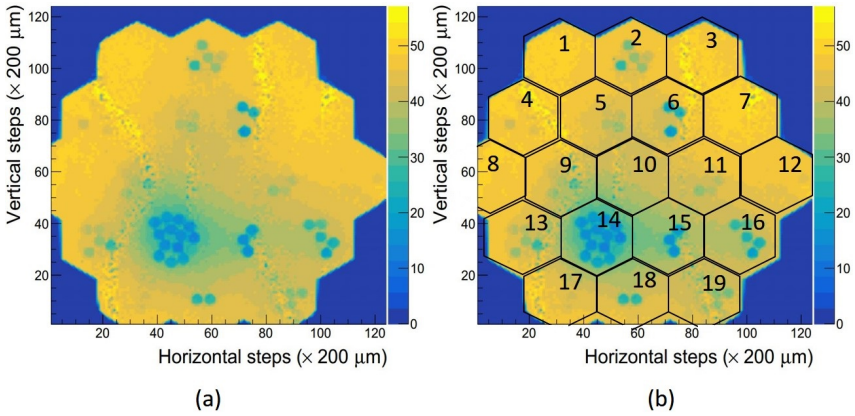

Figure 9: a) Scan of full HPD surface [1], b) Pixel arrangement of this HPD [1]

A full surface scan of this HPD had been done in the earlier study to analyze the condition of the photocathode.[1] It was done with a step size of 200 μm along transverse axes. Figure 9 shows the 2D histogram of the position dependent current response of the photocathode. The current distribution on the surface was found to be non-uniform and some extremely fine, circular regions registered very low currents (damaged regions). Figure 9 shows that pixel 14 is highly damaged region. There are 13 spots in pixel 14 which registered very low current, which is also the number of fibers that were mapped onto pixel 14 (Figure 2(b)). This observation supports the hypothesis that the damage to the photocathode is caused by the scintillation light brought by optical fibers and the circular spots were formed due to excessive illumination by optical fibers.

To analyze the damaged regions microscopically, localized surface scans of the damaged pixels were done with a step size of 75 μm. Pixel number 5, 11, 13, 14, and 18 were scanned and the % loss of signal was measured by comparing the mean current in the damaged region with the mean current in undamaged region of pixel. Mean current in the undamaged region was found in the following way. Some points were chosen in the undamaged region of pixel and the current in the circular region of a particular radius was averaged out for each chosen point. Then the current calculated for these points was

averaged to find the mean current in the undamaged region of the pixel. The coordinates of the chosen points and the corresponding radius in each pixel are mentioned in table 3. The average current in the fiber imprints was averaged out in a circular region of radius = 5 units (radius of fiber imprint).

Figure 10 shows the 2D histogram of position dependent current recorded in pixel 14. The numbers in the fiber imprints represent the scintillator layer number corresponding to that optical fiber. The fiber mapping is available only for pixel number 14. The mapping of the fibers is done by Optical Decoding Unit and it is not made available in public domain.

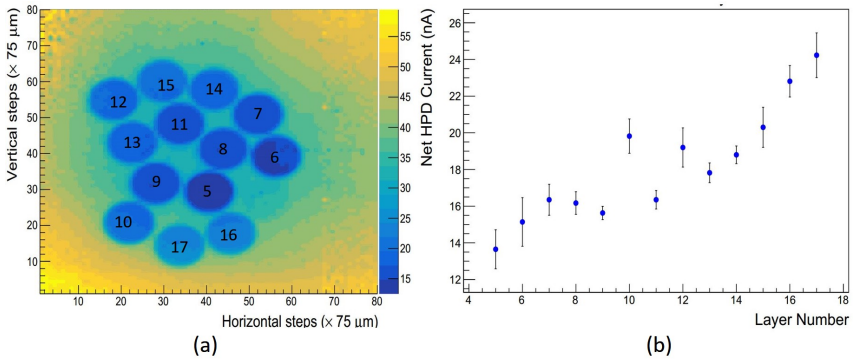

Figure 10: a) Surface scan of pixel 14 (numbers refer to the scintillator layer number corresponding to the optical fiber), b) Variation of net HPD current with layer number

Result of surface scan of other pixels is shown in Figure 11, where, A, B, etc are just the labels of the fiber imprints. These do not correspond to the scintillator layer numbers. The current in fiber imprints of all the scanned pixels and the corresponding % signal loss is mentioned in Table 4.

Comparison of signal loss in pixels

Table 5 shows the observed signal loss in the pixels. The values for signal loss in tower number 2, 6, 15, and 16 have been taken from earlier study.[1]. They have been included here for comparison. The damage is expected to increase with increasing illumination of phototocathode. Following that trend, Pixel 5 (tower 24r) and Pixel 18 (tower 28m) showed less damaged as compared to pixel 2 (tower 24f) and pixel 6 (tower 28f) respectively. But, the damage in pixel 14 was higher than that in both pixel 6 and pixel 18. The justification for this behaviour is following. Since the tower 28 lies very close to the beam

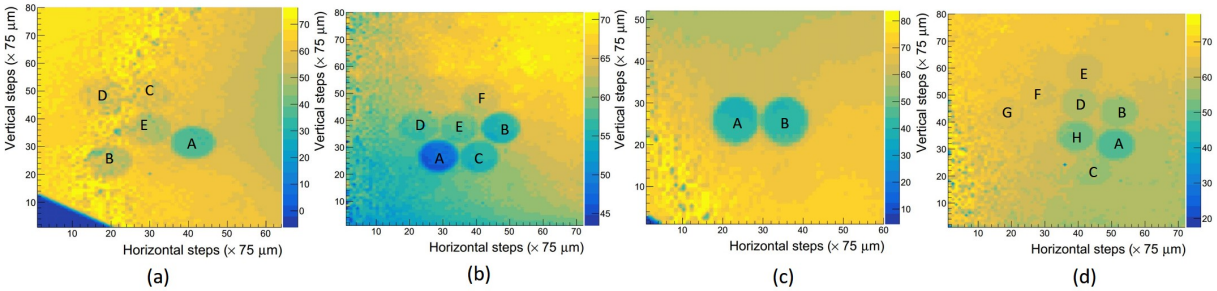

Figure 11: Surface scans of a) pixel 13, b) pixel 11, c) pixel 18, d) pixel 5

Point	Radius (× 75 μm)	No. of Readings	Mean Current (nA)	Std. Dev. (nA)
Pixel 14				
(1,1)	10	111	50.9	4.9
(79,1)	20	355	46.6	3.7
(1,79)	20	355	43.3	3.5
(79,79)	30	736	44.8	4.0
Mean			46.4	4.0
Pixel 13				
(1,78)	25	567	64.0	1.0
(62,1)	20	376	60.0	1.6
Mean			62.0	1.3
Pixel 11				
(1,70)	40	1705	62.9	2.0
(70,1)	35	1070	61.4	2.5
(70,78)	30	797	68.5	0.8
Mean			64.3	1.9
Pixel 18				
(1,50)	22	447	66.6	3.9
(30,1)	20	688	71.1	2.6
(50,59)	20	279	61.6	1.8
(59,1)	25	541	71.2	1.6
Mean			67.6	2.5
Pixel 5				
(1,1)	35	1070	61.1	2.7
(1,70)	35	1357	68.2	1.1
(70,78)	20	567	63.9	1.5
Mean			64.4	1.8

Table 3: Net HPD current recorded in the undamaged region

axis, it collects a huge amount of radiation. Pixel 14 had fibers coming from 13 layers of tower 28. A study by Priscilla Cushman and Brian Sherwood [4] shows that the damage to the photocathode spreads to the neighboring regions. The spread of damage is usually small but in case of pixel 14 the damage in the fiber imprints is very high, therefore, the spread of damage to neighboring regions is also significant. Therefore, the total damage in the pixel 14 was observed to be higher than that of pixel 6 and pixel 18.

7 Threshold Voltage Analysis

Threshold voltage of HPD is defined as the minimum voltage that should be applied across the 3.3 mm gap such that the PIN diodes produce a significant amount of output current. Beyond this voltage, current increases linearly with over voltage. When a photon is incident on the surface of the photocathode, an electron is emitted which is accelerated across the gap by high voltage reverse bias. This electron then hits the PIN diodes and produce secondary carriers which further multiply and produce output current. The damage to photocathode due to excessive illumination by scintillation light was observed.

Fiber Imprint	Mean Current (nA)	Std. Dev.(nA)	% loss
Pixel 14			
L5	13.7	1.1	70.6
L6	15.1	1.3	67.4
L7	16.4	0.8	64.8
L8	16.2	0.6	65.1
L9	15.6	0.4	66.3
L10	19.8	0.9	57.3
L11	16.4	0.5	64.8
L12	19.2	1.1	58.6
L13	17.8	0.5	61.6
L14	18.8	0.5	59.5
L15	20.3	1.1	56.2
L16	22.8	0.9	50.8
L17	24.2	1.2	47.8
Mean			60.8
Pixel 13			
A	36.9	1.6	40.5
B	50.5	4.8	18.6
C	55.8	4.6	10.0
D	56.1	5.6	9.5
E	60.0	2.1	3.1
Mean			16.3
Pixel 11			
A	48.3	2.3	24.9
B	56.0	1.2	12.9
C	56.0	0.9	12.9
D	58.0	1.8	9.7
E	58.2	0.8	9.4
F	63.3	0.9	1.5
Mean			11.9
Pixel 18			
A	40.5	1.6	40.2
B	42.2	1.5	37.7
Mean			38.9
Pixel 5			
A	49.4	0.7	23.3
B	55.5	0.6	13.8
C	56.3	0.8	12.5
D	58.3	0.9	9.4
E	61.1	0.6	5.1
F	63.0	0.7	2.1
G	63.7	1.2	1.1
H	53.0	0.8	17.7
Mean			10.6

Table 4: Mean current recorded and mean % signal loss in all pixels (L denotes scintillator layer)

Pixel	Tower Index	No. of layers	% loss
2	24f	6	25.0
5	24r	12	10.6
6	28f	3	55.0
11	18f	6	11.9
13	22f	6	16.3
14	28r	13	60.8
15	29f	3	59.0
16	26f	6	41.0
18	28m	2	38.9

Table 5: Mean signal loss in pixels

It was expected to manifest in the form of increased threshold voltage in the damaged regions. Therefore, the threshold voltage was measured at different positions over the HPD surface. For damaged region, pixel 14 was chosen as it showed the highest damage among all pixels. Threshold voltage was measured for thirteen points(centers of thirteen fiber imprints) in pixel 14. For the measurement of mean threshold voltage (called as "threshold voltage of undamaged region" in further discussion), twenty five points were randomly chosen on the surface of HPD. The threshold voltage at each point was measured in the following way:

a) PIN diodes were reverse biased by applying -80 V.
b) Dark current was noted.
c) Laser was operated in CW mode (wavelength = 520 nm, frequency = 1kHz, amplitude = 1.6 V, and duty cycle = 99.999%) and the spot on the photocathode was illuminated.
d) The photocathode was reverse biased and the high voltage was ramped up from 0 to -7000V, in the steps of 250 Volts. HPD current was noted at each step.

Figure 12a shows the typical I-V characteristics of HPD. Data generated in earlier study[1] was analyzed to find the threshold voltage. The linear regions of the I-V curve were fitted to straight lines and the threshold voltage was determined by the intersection of these lines. To compare the threshold voltage region in two regions, the result has been shown as a histogram in Figure 12b. The averaged value of observed threshold voltage are -3.405 kV and -3.936 kV for damaged(pixel 14) and undamaged region respectively. Thus the threshold voltage of the damaged region is 531 Volts higher in magnitude than that of undamaged region. Figure 12c shows the variation of conductance in the thirteen fiber imprints of pixel 14. The conductance of photocathode increases with decreasing exposure to scintillation light (i.e. with increasing layer number). It follows the similar trend to that of variation of current with layer number. Thus, the threshold voltage analysis independently characterizes the damage to the photocathode.

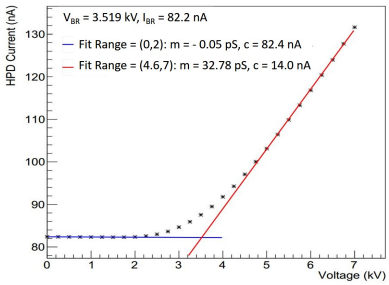

(a) Typical I-V characteristics of HPD

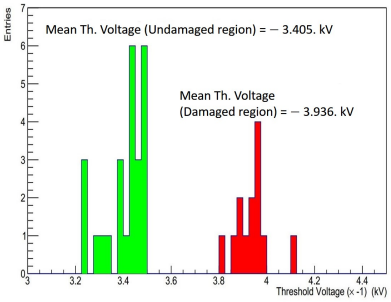

(b) Comparison of threshold voltage in damaged and undamaged regions

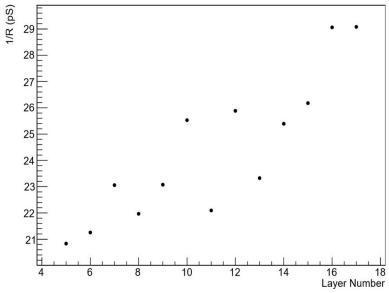

(c) Variation of conductance in fiber imprints of pixel 14

8 Summary and Conclusion

Microscopic characterization of HPD decommissioned from HE detector was carried out using a green laser(wavelength = 520 nm) having beam spot of size between 1.7 μm and 6.2 μm. Before carrying out the surface scans, the focal plane of the laser beam was aligned with the surface of HPD. During the focal plane measurements, rapid variation of current with position was observed due to structure of the fiber optic window when the focal plane of laser beam aligned with the surface of HPD. The characterization of the structure of fiber optic window was carried out with a step size of 1 μm along transverse axes and it was hypothesized that the fiber optic window is made up of square shaped units. The size of one unit was found to be = 6.2 μm. The 2D scans of the damaged region of photocathode were carried out with a step size of 75 μm. The results of the surface scans showed non-uniformity in response of photocathode. Some regions on the photocathode showed significant damage in the shape of circular spots. The damage of photocathode due to scintillation light was already anticipated. The circular spots on the photocathode showed that the damage is more prominent in the region which is covered by the optical fiber than the neighboring regions. Maximum signal loss among the scanned pixels was measured to be = 60.8% in pixel 14. The damage of photocathode was expected to manifest as increase in the magnitude of threshold voltage in damaged regions. Therefore, the threshold voltage was measured at different positions on the photocathode. The magnitude of threshold voltage in the damaged region was found to be 531 V higher than that of undamaged regions. The conductance of photocathode was measured in the damaged region and it was found to be higher in the regions which received less amount of radiation.

Acknowledgements

I thank Prof. Shashi Dugad for his invaluable guidance and support. All the discussions with him were very helpful and motivated me to explore further. I thank Dr. Raghunandan Shukla and Mr. Irfan Mirza for guiding me and helping me throughout the course. I wouldn't have been able to complete this project in the given time without their help in data taking and data analysis process. I thank Prof. Gagan Mohanty for having very informative discussions about CMS detector. I also thank Mr. Ravindra Verma for helping me in data taking, and with the ROOT software.

References

[1] R A Shukla, V G Achanta, P D Barbaro, S R Dugad, A Heering, S K Gupta, I Mirza, S S Prabhu, P Rumerio, "Microscopic Characterisation of Photo Detectors from CMS Hadron Calorimeter". arXiv:1806.09887 [physics.ins-det].

[2] Abdullin, S., Abramov, V., Acharya, B. et al. Eur. Phys. J. C (2008) 55: 159. https://doi.org/10.1140/epjc/s10052-008-0573-y.

[3] Baiatian G. et al.(CMS HCAL Collaboration), "Design, performance, and calibration of CMS hadron endcap calorimeters", CERN-CMS-NOTE-2008-010.

[4] P. Cushman and B. Sherwood, "Lifetime Studies of the 19-channel Hybrid Photodiode for the CMS Hadronic Calorimeter", Tech. Rep. CMS-NOTE-2008-011 (CERN, Geneva, 2007).

[5] R. Shukla, S. Dugad, C. Garde, A. Gopal, S. Gupta, and S. Prabhu, Review of Scientific Instruments 85, 023301 (2014).